COB-2023-0602
INFLUENCE OF THE REAR WING ON SLIDING IN FORMULA 1 VEHICLES

Patrick Ericson da Silva Melo
Leonel R Cancino
Internal Combustion Engines Laboratory - Joinville Technological Center - Federal University of Santa Catarina - LABMCI/CTJ/UFSC.
Rua Dona Francisca 8300, Joinville, SC, CEP 89219-600, Brazil.
hakosho2003@gmail.com
leonel.cancino@labmci.ufsc.br

Abstract. *This work aimed to converge studies of aerodynamics with vehicle dynamics and utilize numerical analysis in CFD (Computational Fluid Dynamics) to investigate the influence of the rear wing on high-performance cars, specifically Formula One cars. The studies conducted for braking and sliding analysis were based on an airfoil profile, namely the NACA 2412, as well as the Drag Reduction System (DRS) mechanism for angle variations ranging from 20º to 0º. Before generating results, mesh refinement was necessary to converge the data for lift coefficient, drag coefficient, and pitch moment. The adopted vehicle dynamics model for the study was the quasi-static model, and flow analysis was conducted to investigate the influence of the rear wing on the vehicle body. The braking situation occurred on a hypothetical straight, flat track without crosswinds, and the sliding situation occurred on the Monza track at the La Parabolica curve, also considered flat and without crosswinds. The software used for the analysis included commercial software like SolidWorks™ for generating CADs of the rear wings, ANSYS FLUENT™ for mesh generation and obtaining aerodynamic load data, and finally Python for importing the data into Excel, where vehicle dynamics formulas for tire reactions during braking and sliding were implemented.*

Keywords: *High performance vehicle, Stability , Braking, Sliding, Aerodynamic loads, Drag Reduction System, CFD.*

1. INTRODUCTION

In the year 1950, the main event of car racing competition began, where the FIA brought together the largest companies in motorsport to form teams for the first official Formula 1 race. During this same period, F1 engines transitioned from small engines, 1.5 L with low power, to 3 L engines with power reaching up to 450 horsepower Motorsport (2018). At the time, the lack of traction and grip on the tires due to increased speed resulted in longer lap times and slower turns due to car instability. Consequently, with the urgency to develop new technologies to improve efficiency, performance, and primarily the stability of F1 cars in corners, as mentioned by Motorsport, the first innovations in the field of aerodynamics in F1 began. In 1968, Colin Chapman implemented the first rear wing on the Lotus 49 at the Monaco Grand Prix. In the following years, with the development of sophisticated wind tunnels and the utilization of computational fluid mechanics for modeling wing geometries suitable for cars, along with the development of optimal airfoil profiles, aerodynamic solutions for vehicles competing in F1 were initiated. Research on the influence that the rear wing has in generating downforce and consequently increasing the stability of high-performance cars can be seen in Katz (1996), through the iteration of the wing with components for two different high-performance cars. According to ANAC (2011), an airfoil is a body designed to produce an aerodynamic reaction normal to the direction of relative motion, as in the case of this work, a wing. Initially, its use began in aviation, where it was considered the heart of airplanes Raymer (2018). However, while airfoils in aviation were intended to generate more lift by increasing the angle of attack and thus keep the plane flying, in F1 cars, the objective was to keep them grounded through negative lift or downforce. From this perspective, the objective of this work is to analyze the influences that the rear wing of F1 cars has on braking and sliding, using the technical regulations of FIA of Formula 1 2022 as a reference for wing modeling. The methodology will adopt Computational Fluid Dynamics analysis using ANSYS FLUENT™ , evaluating the flow and obtaining aerodynamic data for the F1-75, the Ferrari vehicle in the 2022 F1 season, with and without the rear wing.

2. THEORETICAL BACKGROUND

2.1 Racing Car Aerodynamics

According to Leal *et al.*, p.53, the airflow passing through a vehicle directly affects all its components, generating a dynamic pressure. Considering a non-inertial vehicle, three types of forces act on it: the weight force, the normal force acting on the tires due to the weight force, and, finally, the pressure force acting on the vehicle due to the airflow, which

increases with the increase in velocity. For Formula 1 cars that constantly operate at high speeds, there is a demand for high performance throughout the race, and therefore, these pressure forces resulting from the airflow require special attention to maintain car stability and ensure the safety of the drivers. According to Leal *et al.*, these forces can be categorized into two types of aerodynamic forces: drag and lift forces.

2.2 Vehicle Dynamics

The effect of high speeds and the ability to carry heavy loads in current vehicles has led designers to increasingly focus on braking or stopping procedures, both in terms of design and maintenance (Leal *et al.*, 2012, p.86). The problem is not just about stopping or reducing the intensity of movement; what is often desired and required is to make a vehicle stop at a specific time and/or at a specific location. This is when the brakes must come into action, and the importance of their efficiency becomes evident. In the context of braking moments, we arrive at the pre-corner situation where high-performance vehicles must be at the correct speed to avoid situations of skidding that could cause the car to lose stability and consequently, not complete the entire course.

3. METHODOLOGY

Given the complexity and cost of some projects, it becomes necessary to use computational tools for numerical analysis before manufacturing the final product. In the case of the rear wing of an F1 car, it is no different, as it aims to enhance the vehicle's performance at high speeds. Understanding the fluid behavior and the forces acting on the entire body of the vehicle is of utmost importance in achieving greater efficiency in designing the rear wing. Therefore, this work will emphasize the numerical analysis aspect.

3.1 Case study

The present study aims to investigate the influence of the rear wing on the stability of F1 cars, focusing on tire reactions during braking and sliding. To accomplish this, a NACA 2412 airfoil and variations of the angle of attack were used, along with a Drag Reduction System (DRS) wing model. The quasi-static model proposed by Leal *et al.* (2012) was chosen, assuming a flat, straight track with no crosswinds. Simulations were conducted under symmetric conditions, with Reynolds numbers (Re) of $1.7x10^6$ and $3.4x10^6$, based in chord lenght of rear wing, to examine the impact of velocity on different angles of attack in terms of the resulting lift coefficient (C_L) and drag coefficient (C_D) values. The simulation results were used to develop mathematical expressions for tire reactions during braking and sliding on the *La Parabolica* track at Monza (Monzanet, 2023). In this study, the analysis of this curve is limited to the simplified sliding model proposed by the research. The track has a 30º incline and a radius of 320m (Projetomotor, 2021). For this study, a simplified F1 F-75 geometry was used, reducing computational costs and addressing geometry errors, and an NACA 2412 airfoil wing with a chord length (c) of 600mm in the region where the DRS operates was modeled. The geometries are shown in Figure 1 and 2, and the conditions adopted for the Excel calculations are presented in Table 1.

Table 1. Model Input Conditions.

m(kg)	P(N)	a(m/s^2)	Q_I	Q_r	cg_x(m)	cg_y(m)
795	7800	7.63	564.25	460.76	2.88	0.57

l(m)	x	a_1	a_2	R_{0I}	R_{0II}	μ_0
3.71	0.49	1.9	1.9	4015	3784	0.85

In table 1, the variables correspond to mass(m), weight(P), acceleration(a), inertia resistance(Q_I), rolling resistance(Q_r), center of gravity on the x axis(cg_x), center of gravity on the y axis(cg_y), distance between the center of the tires(l), proportion of the car's weight between the front and rear axles(x), distance from the front axle to the cgx(a_1), distance from the rear axle to the cgx (a_2), front axle load (R_{0I}), rear axle load (R_{0II}), friction coefficient (μ_0).

In Figure 1, the subfigures are described as follow: (a) Validation Model - This model was used to validate the data according to data reported in the literature, (Katz, 1985, 1996). It does not include the front wing, rear wing, and diffuser. (b) Reference Model - This model was used for calculations and comparison with vehicles that include the rear wing. Unlike the Validation Model, it includes the diffuser and front wing, but no specific airfoil profile was used for the front wing. (c) Model with DRS - This model includes the diffuser, front wing, and rear wing with the DRS activated. No specific airfoil profile was used for the front wing. (d) Model without DRS - This model includes the diffuser, front wing, and rear wing with the DRS deactivated. No specific airfoil profile was used for the front wing.
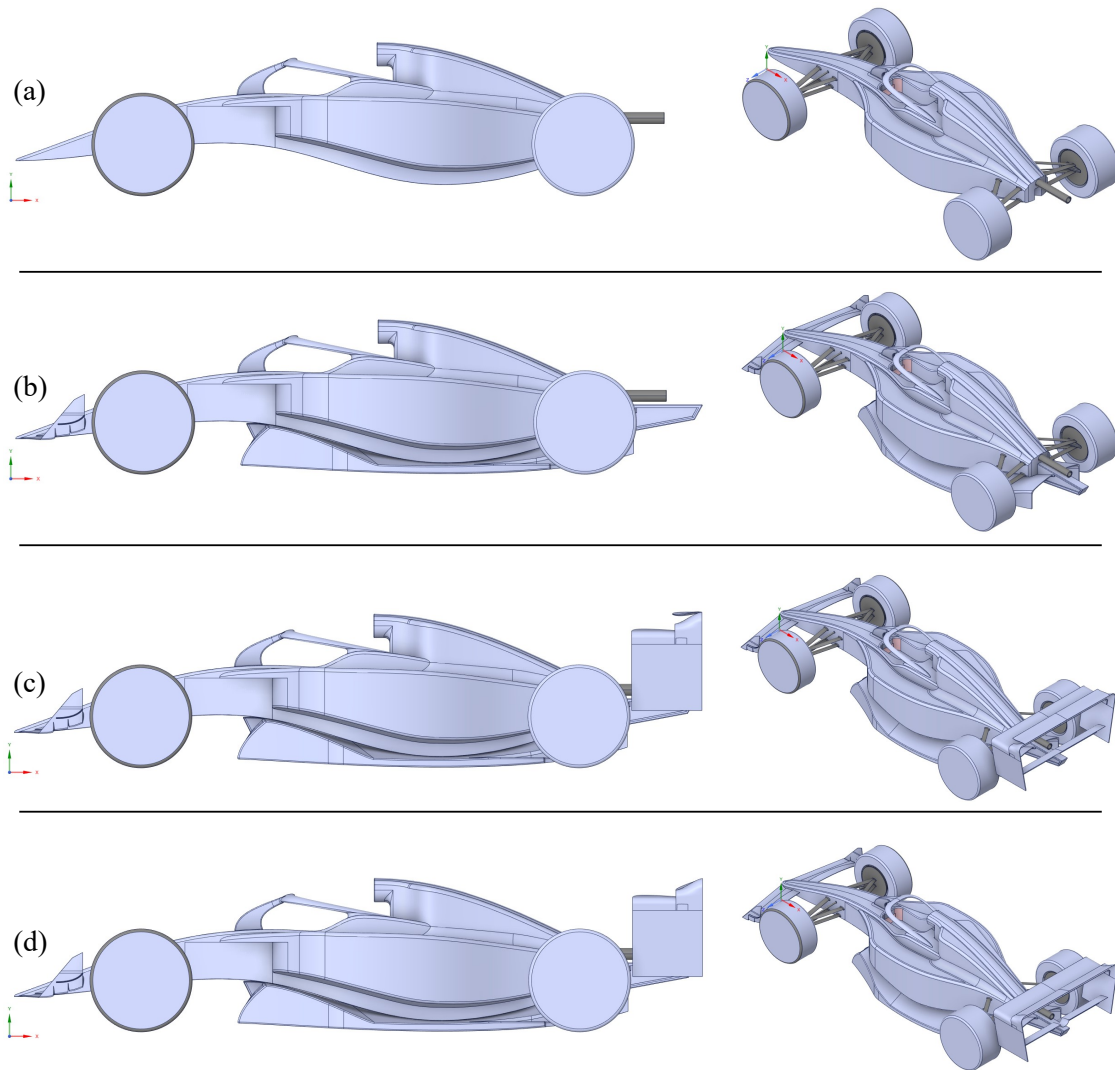
Figure 1. F1 cars geometric models used in this works. (a) Validation Model, (b) Reference Model, (c) Model with DRS, (d) Model without DRS.

3.2 Computational domain and mesh

The computational domain was modeled using the combined geometries of the F1 car and the wing in SpaceClaim, ensuring they were positioned at a sufficient distance to avoid recirculation regions and adverse conditions at the boundaries of the computational domain, thus minimizing numerical errors. Along the mesh generation, some strategies were performed in order to increase the mesh quality. As shown in Figure 3 one control volumes were created.

The blockage ratio is defined as the ratio between the projected area of the model and the test section of the wind tunnel, where Figure 3(a) shows the dimensions adopted for calculating the blockage ratio in this work. When the blockage ratio is increased, the absolute value of the back pressure increases and this directly leads to an increase in the drag coefficient. A study made by Takeda and Kato (1992) also reveals that in the test with a blockage ratio of less than 5%, there are no major blockage effects. Because of this, in the present work the focus blockage ratio was below 5% and was 4.47%.

For mesh generation, the Poly-Hexcore method was used, where Hexcore and Poly-Hexcore meshes are based on meshing technology that applies a hexahedral element to the volume. Hexahedral elements are computationally efficient compared to tetrahedral and polyhedral elements, reducing the element count and saving computational resources without compromising accuracy. The hexahedral element is applied throughout the volume, from the boundary layer region with finer elements, as it is the region of interest that enables precise results, to the outer region of the boundary layer with a growth rate that ensures a smooth transition, as shown in Figure 4..
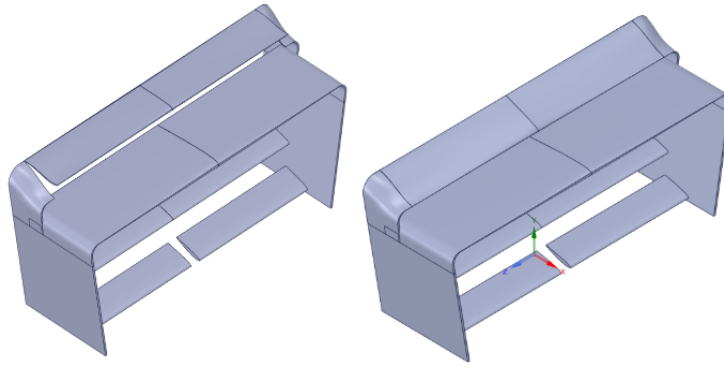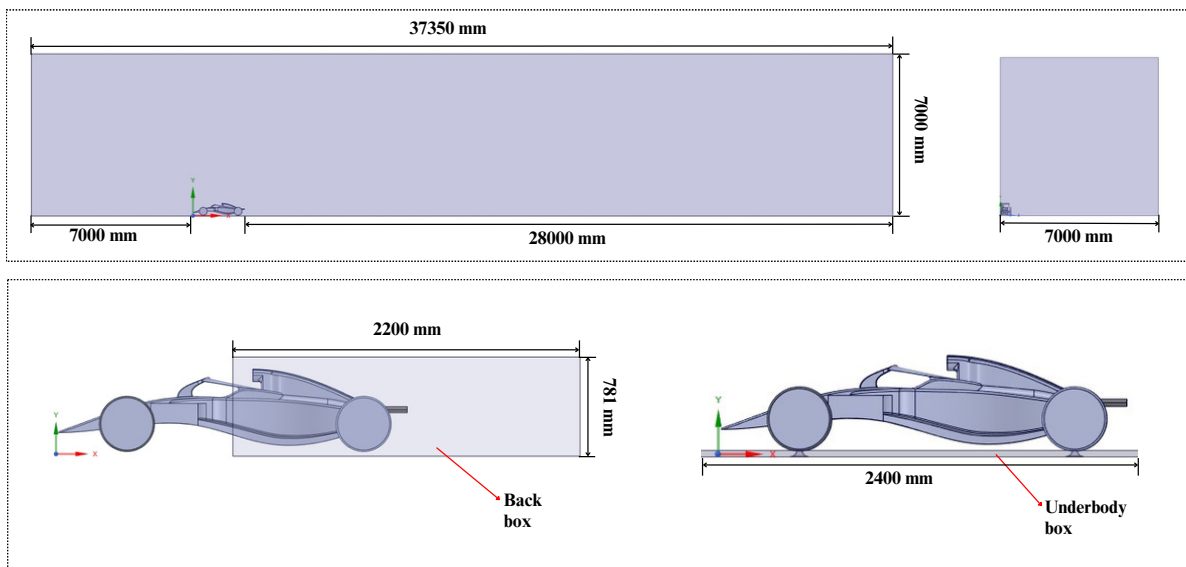
Figure 2. CAD of the Rear Wings.

Figure 3. (a) Wind tunnel virtual test section.

3.3 Model set-up

The chosen solver was based on pressure, as it deals with a constant density analysis (incompressible flow). The velocity formulation used was absolute, disregarding relative velocities outside the system. For numerical analysis works, there are various approaches to solving the Navier-Stokes equations, and this work adopts the methodology for solving the Reynolds-Averaged Navier-Stokes (RANS) equations. According to Wilcox, this model can solve the equations more quickly, but at the expense of some accuracy. The turbulence model adopted was the Realizable k-Epsilon, which will be briefly discussed in this work, but more details can be found in the article by Professor Riley. The term "Realizable" means that the model satisfies certain mathematical restrictions on Reynolds stresses consistent with the physics of turbulent flows, thus providing a more accurate prediction of spreading rates of flat and round jets. The model also outperforms other models for flows involving rotation, boundary layers under strong pressure gradients, separation, and recirculation. Initial studies have shown that the Realizable model provides the best performance among various versions of the k-model for several validations of separated flows and flows with complex secondary flow characteristics. The non-equilibrium wall function was used for regions near walls because it performs better in adverse pressure gradients and can cooperate with fluid separation and attachment to the surface, which is common in aerodynamics of the car. For the vehicle, a scale of 2.4 was adopted in the simulations due to the dimensions of the CAD, the velocity values of 40 m/s correspond to a vehicle moving at 180 km/h, and 80 m/s corresponds to 288 km/h, which are slightly below the average speed of a Formula 1 vehicle that consistently reaches speeds of 300 km/h. A higher velocity value was not chosen to avoid reaching a subsonic regime. It is worth noting that in this simulation, the wheel movement was considered to capture a better flow phenomenology, where the vehicle has stationary walls, and the wheels have non-stationary walls. For external flow, ANSYS FLUENT™ recommends a turbulence intensity of 1% for velocity inlet and 5% for pressure outlet. The
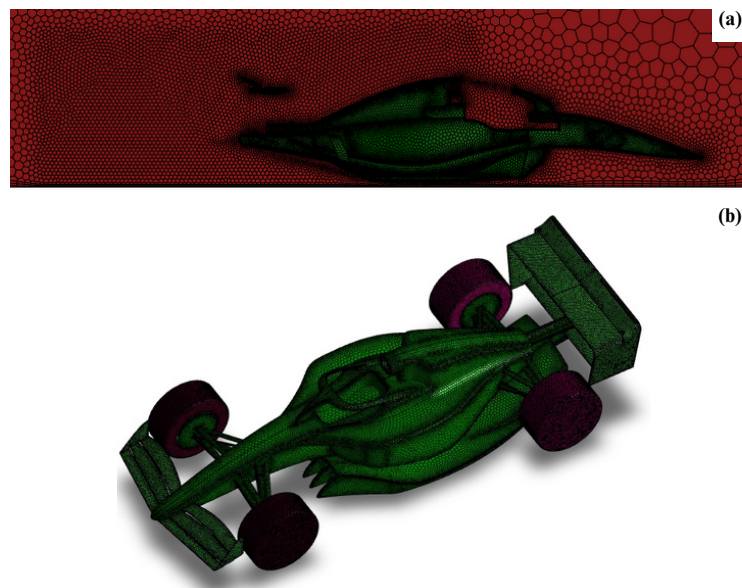
Figure 4. Mesh used in this work.

Figure 5 shows the boundary conditions adopted in the interactions between the wall and the body, other values used for aerodynamic calculations were the frontal area and air density, as shown in Table 2, which presents the adopted boundary conditions in fluent set-up.
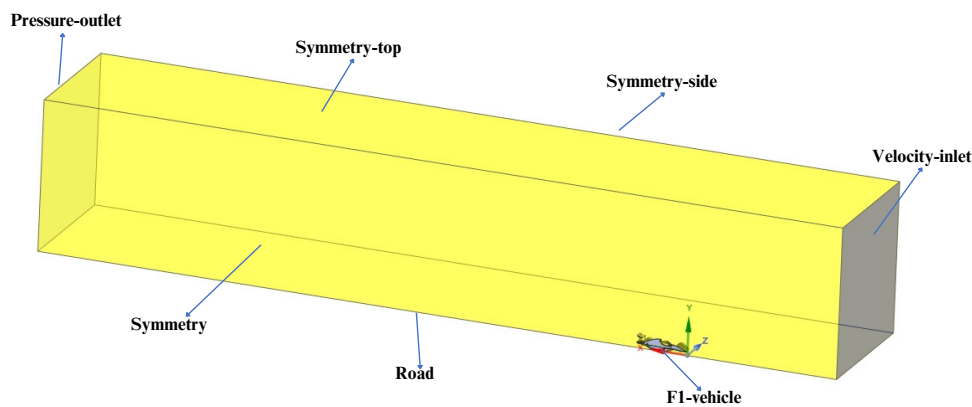

Figure 5. Boundary Conditions.

The chosen initialization method was a hybrid approach, using standard parameters for 10 iterations. After initialization, an average of 700 iterations using first-order equations for momentum, turbulent dissipation rate, and turbulent kinetic energy were performed. The value for the turbulent dissipation rate and turbulent kinetic energy was set to 0.8 and finally, a scale 2.4 times larger was used in ANSYS FLUENT™ due to the reduced dimensions of the CAD when compared to the real F1 vehicles.

3.4 Mesh convergence test

The validation of the model was performed according to the results of reported in the literature (Katz, 1985, 1996). Only Model 3 with the diffuser was used for data validation, as this study did not involve the front wing, making it impossible to compare with the other models. It was assumed that the geometry and velocity adopted in the CAD and simulation would be similar to those of the reference model.

For validation, five meshes with varying levels of refinement were created. Due to the complex geometry of the F1 car, a low-refinement mesh could not be used as it resulted in errors during mesh generation. By observing the graphs in Figure 6 and 7, it can be seen that the data generated by ANSYS FLUENT™ closely aligns with the reference data. Despite the discrepancy in the number of elements, there is not a significant variation in the values of C_L and C_D for situations

Table 2. Boundary Conditions.

F1 Vehicle	Wheels	Interior	Outlet	Inlet
Stationary wall / Viscous Forces	174 rad/s 348 rad/s	Air Flow	Turbulence intensity 5% Turbulent viscosity rate = 10	40 m/s 80 m/s Turbulence intensity 1%

involving analysis based on DRS, which also validates the efficiency of the Poly-Hexcore meshing element in achieving data convergence and the performance of the chosen turbulence model. The graphs below also show the convergence of data for the different mesh refinements in the F1 car geometries combined with the wing and two angles of attack in the DRS.
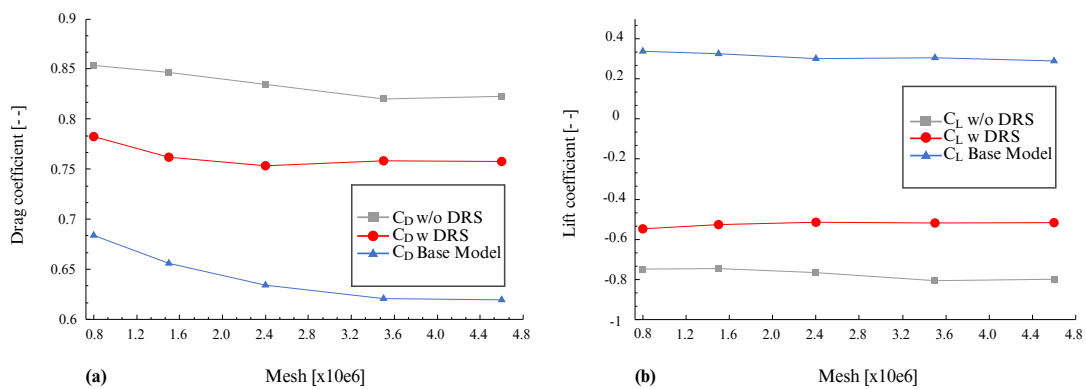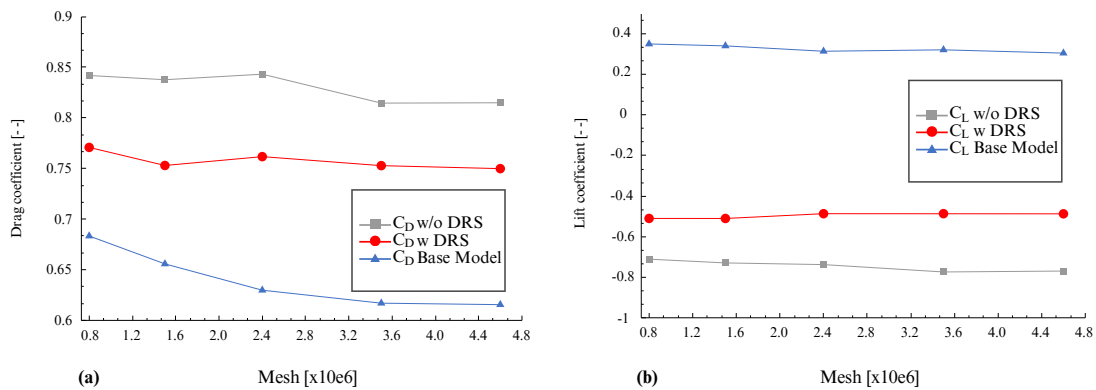

Figure 6. c_L and c_D at $Re_L = 1.7\text{x}10^6$.

Figure 7. c_L and c_D at $Re_L = 3.4\text{x}10^6$.

4. RESULTS AND DISCUSSIONS

The results were divided into three stages. The first stage focused on analyzing the effects of the rear wing on the vehicle's flow, the second stage demonstrated these effects on vehicle dynamics during braking, and the third stage simulated a sliding situation in a curve. The second and third stages aimed to replicate the profiles of the vehicles used in this study.

4.1 Wing – body interaction

As the essence of the work is to assess the influence of the rear wing on the stability of F1 vehicles during braking, it was necessary to initially analyze the behavior of the flow lines with and without the rear wing to determine where the

aerodynamic forces originate from that will affect the tire reactions. This result demonstrates the expected flow separation behavior, where, according to Katz, the interaction between the wing and the body will enhance aerodynamic effects, with the primary expectation being an increase in downforce. In the analysis of flow, the velocity profile results are examined to verify the principle of Bernoulli, where an increase in pressure along a streamline should correspond to a decrease in velocity at a certain point, and vice versa. Raymer (2018). Figure 8 demonstrate this relationship. Thus, the passage of the vehicle with the wing causes the air to move differently over the vehicle surface, resulting in increased skin friction drag and a modification in the velocity distribution of the particles in the domain, altering the pressure distribution Raymer (2018), and ultimately generating negative lift.
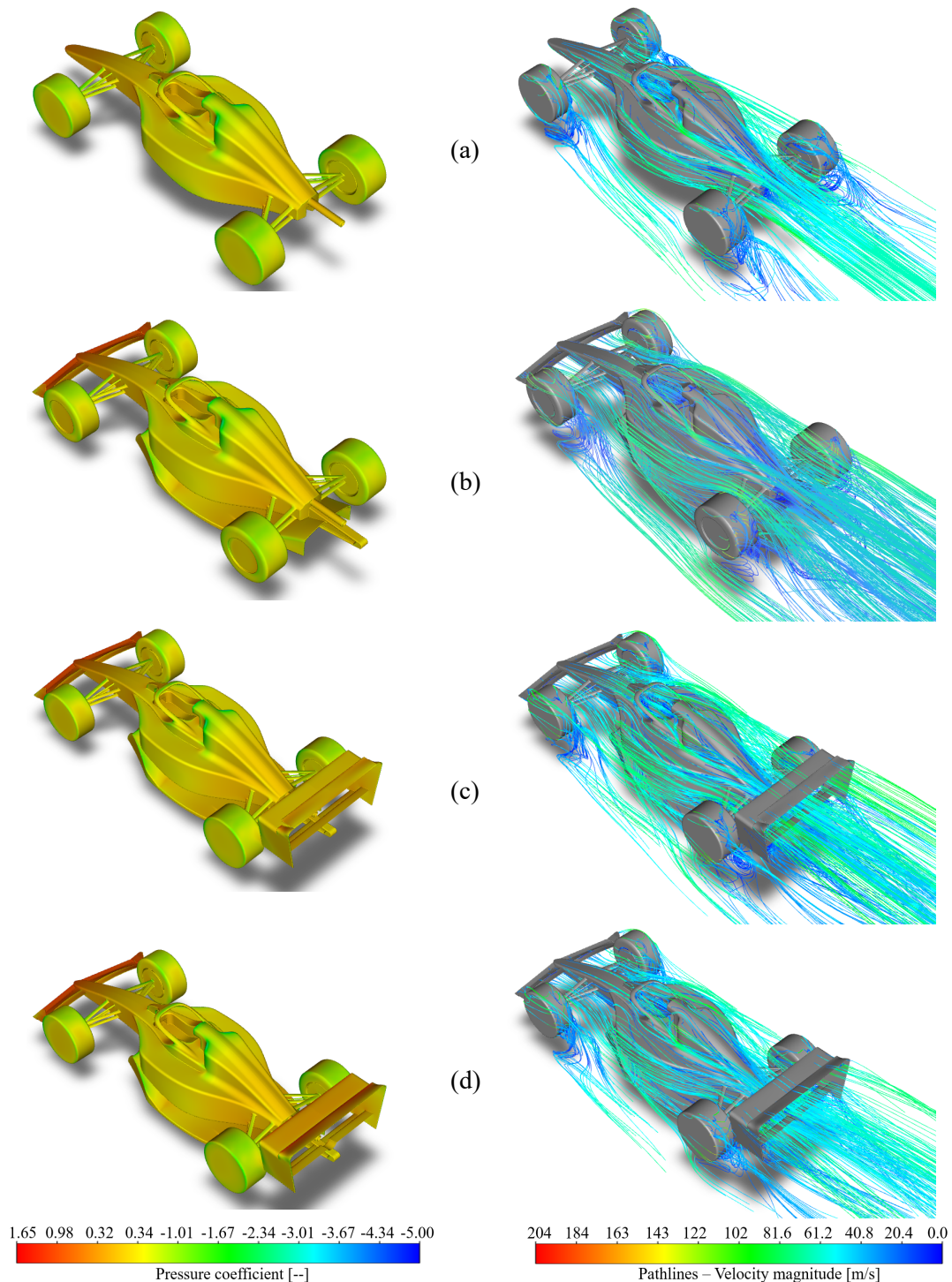

Figure 8. Pressure coefficient and pathlines for $\text{Re}_L = 3.4\text{x}10^6$. (a) Validation Model, (b) Reference Model, (c) Model with DRS, (d) Model without DRS.

4.2 Pressure coefficient

Further analysis was conducted to study the distribution of pressure coefficient throughout the domain, as depicted in Figure 8. In the region of the rear wing, Figure 9, the expected behavior of an inverted airfoil is evident, clearly showing areas of high and low pressure. For the rear wing without DRS activation, there is a greater pressure difference, which, according to Raymer (2018), can be attributed to the airflow path over the airfoil. In the case of the symmetrical NACA2412 airfoil, its curvature should not induce high negative lift values. In the geometry of Figure 8, the flow of particles is significantly reduced, further highlighting the influence of the rear wing on the number of particles passing through that region. Figure 9 provides a more detailed demonstration of the specific region of the rear wing and the pressure and velocity gradients.
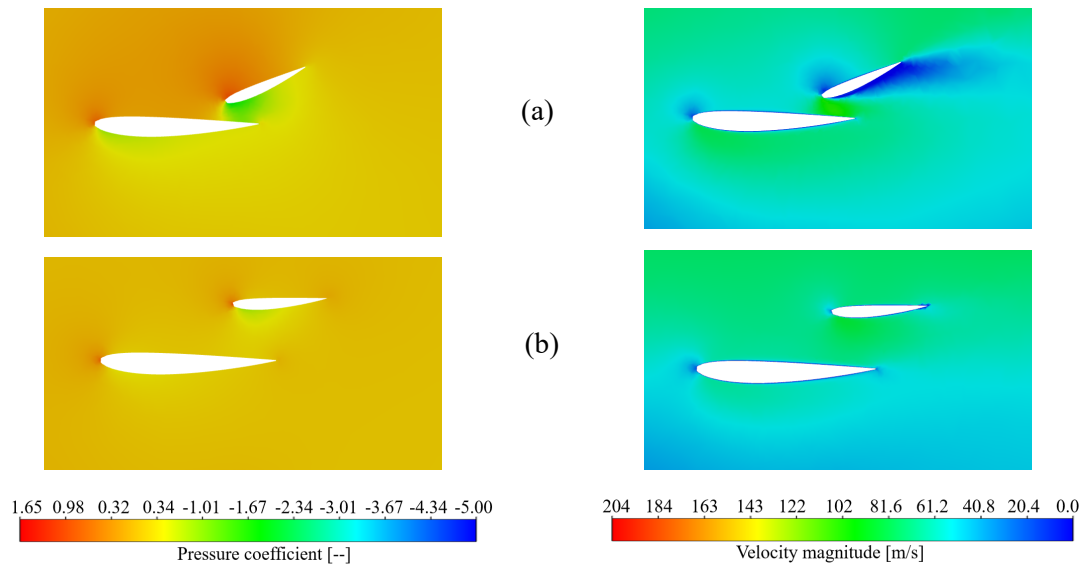

1.65 0.98 0.32 0.34 -1.01 -1.67 -2.34 -3.01 -3.67 -4.34 -5.00
Pressure coefficient [--]

204 184 163 143 122 102 81.6 61.2 40.8 20.4 0.0
Velocity magnitude [m/s]

Figure 9. Pressure coefficient and velocity fields for $Re_L = 3.4 \times 10^6$. (a) Model with DRS, (b) Model without DRS.

4.3 Tire reactions for braking and sliding

Considering that the objective of this study is to identify the relationship between the wing and vehicle stability during braking and sliding situations, Tables 3 and 4 present the results of the aerodynamic forces, while Tables 5 and 6 provide the tire reactions during braking and the required braking force for the vehicle at specific velocities.

Table 3. Lift and Drag at $Re_L = 1.7 \times 10^6$.

Type	L (kN)	D (kN)	M_L (kN.m)
Base model	-0.62	1.53	-0.52
DRS	-1.11	1.63	-0.86
n-DRS	-1.60	1.64	-2.34

Table 4. Lift and Drag at $Re_L = 3.4 \times 10^6$.

Type	L (kN)	D (kN)	M_L (kN.m)
Base model	-2.38	6.18	-2.17
DRS	-4.20	6.46	-3.37
n-DRS	-6.16	6.52	-9.01

The Tables 3 and 4, which demonstrate two different velocity scenarios and their influence on aerodynamic forces, confirm the expected results due to the fluctuation of pressure coefficient in the aforementioned regions. Consequently, there is an increase in negative lift and drag forces on both the wing and the body. Another interesting aspect to analyze is the difference in negative lift compared to drag based on the angle of attack, considering the activation or deactivation of the DRS system. When the DRS is activated, corresponding to a 0° angle of attack, there is a decrease in wetted area and, due to the symmetry of the airfoil curvature, a relative increase in lift and drag. On the other hand, when the DRS is deactivated, there is an increase in drag due to the pressure caused by high acceleration at the leading edge, where the boundary layer is thicker, followed by its reduction and deceleration along the geometry until the flow reversal point. As a result, there is a slight increase in drag due to pressure, as well as a more considerable increase in negative lift due to the increased angle of attack. These trends are depicted in the graphs shown in Figures 6 and 7. As for the braking situation, the expected load distribution is observed, with a front-to-rear bias of approximately 0.51 and 0.49, respectively, and a transfer of weight from the rear to the front during braking. This is consistent with the stability requirements of a

four-wheel braking system, as mentioned in the case study, Tables 5 and 6. It is worth noting that in the situation where the DRS is deactivated, there is a sudden shift in the CP position along the x-axis, resulting in a greater influence on pitch moment due to the increased negative lift and consequently, there is a significant increase in pitch moment for the condition without DRS activation.

Table 5. Tire Reactions and Braking at $\text{Re}_L = 1.7\text{x}10^6$.

Type	R_f (kN)	R_a (kN)	F_f (kN)	a (m/s^2)
Base model	4.34	4.11	7.18	11.39
DRS	4.62	4.33	7.60	12.03
n-DRS	5.26	4.16	8.01	12.56

Table 6. Tire Reactions and Braking at $\text{Re}_L = 3.4\text{x}10^6$.

Type	R_f(kN)	R_a(kN)	F_f(kN)	a(m/s^2)
Base model	5.07	5.14	8.67	19.39
DRS	6.26	5.77	10.23	23.72
n-DRS	8.67	5.32	11.88	23.88

The average speed at the *La Parabolica* curve in Monza is 55 m/s, whereas the calculations in this study are based on velocities of 40 m/s and 80 m/s. According to the maximum speed model for stable cornering without slipping proposed by Leal *et al.* (2012), the maximum speed at *La Parabolica* is 52 m/s. Therefore, considering that this study did not focus on maximizing negative lift generation through specific airfoil profiles, nor did it address the front wing and diffuser, the results obtained are coherent. They demonstrate a complete loss of stability for the 80 m/s scenario and a partial loss of stability for the 40 m/s scenario. Additionally, the results highlight the reduced performance of the vehicle when no influence from the rear wing is present, Tables 7 and 8.

Table 7. Sliding at $\text{Re}_L = 1.7\text{x}10^6$.

Type	e(%)
Base model	47.2
DRS	44.6
n-DRS	42.3

Table 8. Sliding at $\text{Re}_L = 3.4\text{x}10^6$.

Type	e(%)
Base model	153.6
DRS	132.4
n-DRS	113.9

5. CONCLUSIONS

Fluid simulations in the automotive industry are of great importance, providing good results with much lower cost and time compared to real testing, such as using a wind tunnel for vehicle aerodynamics. Knowing how to develop a good mesh, making the most of the available computational effort, and correctly applying boundary conditions related to fluid mechanics, as well as turbulence models, will yield satisfactory results in simulating the specific problem. This aims to reduce costs and avoid issues in the production of future products, as well as enhance their efficiency.The present study aimed to provide a case study on the influence of the rear wing on braking and sliding situations in F1 cars, combining the fields of aerodynamics and vehicle dynamics. It illustrated the computational and physical processes involved in such an investigation. Understanding these processes allowed for a better comprehension of control volume concepts, conservation of mass and momentum, velocity and pressure field and relationships at different points in the domain, and how they affect the path field. In addition, he emphasized the importance of a well-developed CAD model, both in simplification and in the correction of bugs involving edges to generate meshes that do not have topology problems. Also, the need for advanced techniques proposed by each element in the simulations to ensure convergence in more complex geometries was understood. These efforts ultimately contribute to obtaining better results in high-impact scenarios, such as braking and sliding at high speeds in this study.

Using the Quasi-Static model proposed by Leal *et al.* (2012), the obtained results demonstrated that the scenario where the DRS is deactivated is more favorable for braking and skidding situations, as it shows a greater influence of aerodynamic forces with varied angles of attack on the DRS of the rear wing compared to the model with the DRS activated. Regarding sliding situations, it is important to highlight the significance of studying yaw moments in specific scenarios, as it allows for a more comprehensive analysis of the car's performance during curves. In this study, it is worth noting that the utilized model, even though simplified in some aspects, was of utmost importance in understanding crucial concepts in Formula 1 racing. The author of this work acknowledges that the use of the Quasi-Static model with computational analysis in the F-75 CAD to obtain aerodynamic loads and calculate braking and skidding situations can open doors for more dynamic and interactive studies involving both racing teams and scientific research, aiming for a better understanding and knowledge of high-performance cars for the Brazilian automotive scenario.

Furthermore, the study identified the importance of a thorough analysis of the airfoil profile to achieve improved or reduced performance in the wing design. As mentioned by Raymer (2018), the choice of airfoil profile is not based on pre-existing profiles but rather generated according to the specific project requirements. This opens up avenues for future research focusing on airfoil profiles as a case study.

6. ACKNOWLEDGEMENTS

7. REFERENCES

ANAC, 2011. "Aerofólio". URL `https://www2.anac.gov.br/anacpedia/por_ing/tr428.htm`.

FIA, 2022a. "2022 fia formula one world championship". URL `https://www.fia.com/events/fia-formula-one-world-championship/season-2022/2022-fia-formula-one-world-championship`.

FIA, 2022b. "2022 formula 1 technical regulations". URL `https://www.fia.com/sites/default/files/2022_formula_1_technical_regulations_-_iss_3_-_2021-02-19.pdf`.

Katz, J., 1985. "Investigation of Negative Lifting Surfaces Attached to an Open-Wheel Racing Car Configuration". SAE Technical Paper 850283, SAE International, Warrendale, PA. doi:10.4271/850283. URL `https://www.sae.org/publications/technical-papers/content/850283/`. ISSN: 0148-7191, 2688-3627.

Katz, J., 1996. *Race Car Aerodynamics: Designing for Speed*. Bentley Publishers, Cambridge, MA, USA, 2nd edition. ISBN 978-0-8376-0142-7.

Leal, L., da Rosa, E. and Nicolazzi, L., 2012. "Uma introdução à modelagem quase–estática de automóveis". Technical report, UFSC, Florianápolis.

Monzanet, 2023. "Autodromo nazionale monza". URL `https://www.monzanet.it/`.

Motorsport, U., 2018. "The first appearance of wings on formula 1 cars". URL `https://us.motorsport.com/f1/news/1968-first-wings-f1-1000902/1389076/`.

Projetomotor, 2021. "A história das incríveis curvas inclinadas de monza". URL `https://projetomotor.com.br/f1-historia-curvas-inclinadas-monza/`.

Raymer, D.P., 2018. *Aircraft Design: A Conceptual Approach*. American Institute of Aeronautics & Ast., Reston, VA, 6th edition. ISBN 978-1-62410-490-9.

Riley, J., 2006. "Advanced turbulence modeling techniques". URL `https://courses.washington.edu/mengr544/handouts-10/Fluent-k-epsilon.pdf`.

Takeda, T. and Kato, M., 1992. "Wind tunnel blockage effects on drag coefficient and wind-induced vibration". In *Vol. 42*. J. Wind Eng. Ind. Aerody, pp. 897–908. URL `https://www.sciencedirect.com/science/article/abs/pii/016761059290096S?via%3Dihub`.

Wilcox, D., 1988. "Reassessment of the scale-determining equation for advanced turbulence models". *AIAA Journal*, Vol. 26, No. 11, pp. 1299–1310.

8. RESPONSIBILITY NOTICE